Pseudo-spin Symmetry and Relativistic Single-nucleon Wave Functions

Joseph N. Ginocchio* and David G. Madland†

Theoretical Division, Los Alamos National Laboratory

Los Alamos, NM 87545

Abstract

We show that the occurrence of approximate pseudo-spin symmetry in nuclei is connected with certain similarities in the relativistic single-nucleon wave functions of the corresponding pseudo-spin doublets. We perform a case study in which several examples and the systematics of this connection are explored.

PACS numbers: 24.10.Jv, 21.60.Cs, 21.10.-k, 24.80+y.

I. INTRODUCTION

In a recent paper [1] it was shown that quasi-degenerate pseudo-spin doublets in nuclei, discovered almost thirty years ago [2,3], arise from the near equality in magnitude of attractive scalar, V_S, and repulsive vector, V_V, relativistic mean fields, $V_S \sim -V_V$, in which the nucleons move. Pseudo-spin doublets have non-relativistic quantum numbers (n_r, ℓ,$j = \ell + 1/2$) and ($n_r - 1, \ell + 2$, $j = \ell + 3/2$) where n_r,ℓ, and J are the single-nucleon radial, orbital, and total angular momentum quantum numbers, respectively. These authors defined a "pseudo" orbital angular momentum $\tilde{\ell} = \ell + 1$; for example, $(n_r s_{1/2}, (n_r - 1)d_{3/2})$ will have $\tilde{\ell} = 1$, $(n_r p_{3/2}, (n_r - 1)f_{5/2})$ will have $\tilde{\ell} = 2$, etc. Then these doublets are almost degenerate with respect to "pseudo" spin, $\tilde{s} = 1/2$, since $j = \tilde{\ell} \pm \tilde{s}$ for the two states in the doublet. This symmetry has been used to explain a number of phenomena in nuclear structure [4] including most recently the identical rotational bands observed in nuclei [5], and to establish an effective shell model coupling scheme [6]. A near equality in the magnitude of mean fields seems to be a universal feature of relativistic theories ranging from relativistic field theories with interacting nucleons and mesons [7], to nucleons interacting via Skyrme-type interactions [8,9], to QCD sum rules [10]. In this paper we investigate the consequences of $V_S \sim -V_V$ on the single-nucleon wave functions. The connection between the Dirac equation and pseudo-spin symmetry is reviewed in Sec. II. The relativistic mean field model described in Sec. III is used for the calculations of the case study presented in Sec. IV. Our conclusions are given in Sec. V.

II. THE DIRAC EQUATION AND PSEUDO-SPIN SYMMETRY

The Dirac equation with external scalar, V_S, and vector, V_V, potentials is given by:

$$[c\alpha \cdot p + \beta(mc^2 + V_S) + V_V]\Psi = \mathcal{E}\Psi, \tag{1}$$

where α and β are the usual Dirac matrices [11]. We shall be considering relativistic mean field theory with spherical symmetry for which the scalar and vector potentials de-

pend only on the radial coordinate. In this case the orbital angular momentum is not a conserved quantum number in general. Instead a nucleon moving in a spherical relativistic field is labeled by a radial quantum number, n_r, total angular momentum j, its projection on the z-axis, m, and $\hat{\kappa} = -\beta(\hat{\sigma} \cdot \hat{L} + 1)$ [11]. The eigenvalues of $\hat{\kappa}$ are $\kappa = \pm$(j + 1/2); – for aligned spin ($s_{1/2}, p_{3/2}$, etc.) and + for unaligned spin ($p_{1/2}, d_{3/2}$, etc.). Thus, the quantum number κ and the radial quantum number n_r are sufficient to label the orbitals. The spherically symmetric Dirac wave function can then be written in terms of upper and lower components $\Psi_{\kappa>0,m} = (g_\kappa[Y_\ell \chi]_m^{(j=\ell-1/2)}, i f_\kappa[Y_{\ell-1}\chi]_m^{(j=\ell-1/2)})$, $\Psi_{\kappa<0,m} = (g_\kappa[Y_\ell \chi]_m^{(j=\ell+1/2)}, i f_\kappa[Y_{\ell+1}\chi]_m^{(j=\ell+1/2)})$ where g_κ, f_κ are the radial wave functions (omitting the radial quantum numbers), Y_ℓ are the spherical harmonics, χ is a two-component Pauli spinor, and $[\ldots]^{(j)}$ means coupled to angular momentum j. The radial Dirac equation for the upper and lower components (g_κ, f_κ) of the single-nucleon radial wave function in dimensionless units (also omitting the magnetic quantum numbers) is then given by [11]

$$\left[\frac{d}{dr} + \frac{1+\kappa}{r}\right] g_\kappa = \ [2 - E - V(r)\ ] f_\kappa \tag{2}$$

$$\left[\frac{d}{dr} + \frac{1-\kappa}{r}\right] f_\kappa = \ [E + \Delta(r)\ ] g_\kappa, \tag{3}$$

where r is the radial coordinate in units of $\hbar c/mc^2$, $V(r)$ = [$V_V(r)$ - $V_S(r)$] / mc^2, $\Delta(r)$ = [$V_S(r)$ + $V_V(r)$] / mc^2, and E is the binding energy [$E = (mc^2 - \mathcal{E})/mc^2 > 0$] of the nucleon in units of the free nucleon mass. First we repeat the proof [1] that, in the limit of equality of the magnitude of the vector and scalar potential, $\Delta(r) = 0$, pseudo-spin is exactly conserved. To do this, we solve for g_κ in (3) and substitute into (2), obtaining the second order differential equation for f_κ,

$$\left[\frac{d^2}{dx^2} + \frac{2}{x}\frac{d}{dx} - \frac{\tilde{\ell}(\tilde{\ell}+1)}{x^2} \ + (V(r) - 2 + E)\right] f_\kappa = 0, \tag{4}$$

where $x = \sqrt{E}\ r, E \neq 0$, and

$$\tilde{\ell} = \kappa - 1,\ \kappa > 0\ ;\ \tilde{\ell} = -\kappa,\ \kappa < 0, \tag{5}$$

which agrees with the original definition of the pseudo-orbital angular momentum [2,3]. For example, for $(n_r s_{1/2}, (n_r-1)d_{3/2})$, $\kappa = -1$ and 2, respectively giving $\tilde{\ell} = 1$ in both cases. Furthermore, the physical significance of $\tilde{\ell}$ is revealed; it is the "orbital angular momentum" of the lower component of the Dirac wave function and, in this limit, it is a conserved quantum number.

For $E \neq 0$, Equation (4) is a Schrödinger equation with an attractive potential V and binding energy $2 - E$ which depends only on the pseudo-orbital angular momentum, $\tilde{\ell}$, through the pseudo - rotational kinetic energy, $\frac{\tilde{\ell}(\tilde{\ell}+1)}{x^2}$, and not on κ. Hence the eigenenergies do not depend on κ but only on $\tilde{\ell}$. Thus the doublets with the same $\tilde{\ell}$ but different κ ($\kappa = \tilde{\ell}+1$ and $\kappa = -\tilde{\ell}$) will be degenerate, producing pseudo-spin symmetry.

Furthermore, from (4), it is clear that the f_κ with the same $\tilde{\ell}$ can only differ by an overall constant,

$$f_{-\tilde{\ell}} = \mathcal{N}_{\tilde{\ell}}\ f_{\tilde{\ell}+1}. \tag{6}$$

We show now that $\mathcal{N}_{\tilde{\ell}}^2 = 1$. The Dirac wave function is normalized by

$$\int_0^\infty r^2 dr [g_\kappa(r)^2 + f_\kappa(r)^2] = 1. \tag{7}$$

Furthermore, from (3), we find in the pseudo-spin limit,

$$g_{\tilde{\ell}+1}(r) = \frac{1}{E_{\tilde{\ell}}}\left[\frac{d}{dr} - \frac{\tilde{\ell}}{r}\right] f_{\tilde{\ell}+1}(r)\ ,\ g_{-\tilde{\ell}}(r) = \frac{1}{E_{\tilde{\ell}}}\left[\frac{d}{dr} + \frac{\tilde{\ell}+1}{r}\right] f_{-\tilde{\ell}}(r)\ , \tag{8}$$

where we have used $E_{\tilde{\ell}} = E_{\tilde{\ell}+1} = E_{-\tilde{\ell}}$. Using these relations in (7) for both partners, $\kappa = -\tilde{\ell}$ and $\kappa = \tilde{\ell}+1$ and integrating by parts and then using the differential equation (4) for f_κ, we obtain

$$\int_0^\infty r^2 dr f_{\tilde{\ell}+1}(r)^2 (2 - V - 2E_{\tilde{\ell}}) = -E_{\tilde{\ell}},$$

$$\mathcal{N}_{\tilde{\ell}}^2 \int_0^\infty r^2 dr f_{\tilde{\ell}+1}(r)^2 (2 - V - 2E_{\tilde{\ell}}) = -E_{\tilde{\ell}}, \tag{9}$$

which implies that $\mathcal{N}_{\tilde{\ell}}^2 = 1$ for $E_{\tilde{\ell}} \neq 0$. Furthermore, for a square well [1], $\mathcal{N}_{\tilde{\ell}} = -1$ and therefore we assume that this is the case for more realistic nuclear mean fields as well.

As pointed out in [1], there will not be any bound Dirac valence states, only Dirac sea states, for the pseudo-spin limit $\Delta = 0$, which would contradict the fact that bound nuclei exist. In [1] it was shown that it is possible to have bound valence states *and* quasi-degeneracy for a small $\Delta(r)$ by studying the Coulomb potential and the spherical potential well, $V_{s\,,v}(r) = V_{s\,,v} > 0\ ,\ r < R\,;\ V_{s\,,v}(r) = 0\ ,\ r > R$. Likewise, one may ask how well the relation

$$f_{-\tilde{\ell}}(r) = -f_{\tilde{\ell}+1}(r) \tag{10}$$

holds for small pseudo-spin breaking. In this paper we employ a physically more realistic Dirac-Hartree approach to answer this question.

III. RELATIVISTIC POINT COUPLING MODEL

We use a self-consistent Dirac-Hartree model with contact interactions (point couplings) in the mean field ($\psi \longrightarrow \langle\,\psi\,\rangle$) and no Dirac sea approximations. The model consists of four-, six-, and eight-fermion point couplings leading to scalar and vector densities with both isoscalar and isovector components, derivatives of the densities to simulate the finite ranges of the mesonic interactions, but no explicit meson fields. The Lagrangian is given by

$$\mathcal{L} = \mathcal{L}_{free} + \mathcal{L}_{4f} + \mathcal{L}_{hot} + \mathcal{L}_{der} + \mathcal{L}_{em}\ ,\quad \text{where} \tag{11}$$

$\mathcal{L}_{free}$ and $\mathcal{L}_{em}$ are the kinetic and electromagnetic terms, and

$$\begin{aligned}\mathcal{L}_{4f} = &-\frac{1}{2}\alpha_S(\bar{\psi}\psi)(\bar{\psi}\psi) - \frac{1}{2}\alpha_V(\bar{\psi}\gamma_\mu\psi)(\bar{\psi}\gamma^\mu\psi) \\ &-\frac{1}{2}\alpha_{TS}(\bar{\psi}\vec{\tau}\psi)\cdot(\bar{\psi}\vec{\tau}\psi) - \frac{1}{2}\alpha_{TV}(\bar{\psi}\vec{\tau}\gamma_\mu\psi)\cdot(\bar{\psi}\vec{\tau}\gamma^\mu\psi)\ ,\end{aligned} \tag{12}$$

$$\begin{aligned}\mathcal{L}_{hot} = &-\frac{1}{3}\beta_S(\bar{\psi}\psi)^3 - \frac{1}{4}\gamma_S(\bar{\psi}\psi)^4 \\ &-\frac{1}{4}\gamma_V[(\bar{\psi}\gamma_\mu\psi)(\bar{\psi}\gamma^\mu\psi)]^2\ ,\ \text{and}\end{aligned} \tag{13}$$

$$\mathcal{L}_{der} = -\frac{1}{2}\delta_S(\partial_\nu\bar{\psi}\psi)(\partial^\nu\bar{\psi}\psi) \\ -\frac{1}{2}\delta_V(\partial_\nu\bar{\psi}\gamma_\mu\psi)(\partial^\nu\bar{\psi}\gamma^\mu\psi) \ . \tag{14}$$

In these equations, ψ is the nucleon field, the subscripts "S" and "V" refer to the scalar and vector nucleon fields, respectively, and the subscript "T" refers to isovector fields containing the nucleon isospin $\vec{\tau}$. The physical makeup of $\mathcal{L}$ is that $\mathcal{L}_{4f}$ is a four-fermion interaction, while $\mathcal{L}_{hot}$ contains higher order six-fermion and eight-fermion interactions, and $\mathcal{L}_{der}$ contains derivatives in the nucleon densities. There are a total of nine coupling constants.

Minimizing the expectation value of the Hamiltonian corresponding to Eq. (11) in the space of Slater determinants $|\phi\rangle$ leads to the Dirac-Hartree equations containing the following potentials:

$$V_S = \alpha_S\rho_S + \beta_S\rho_S^2 + \gamma_S\rho_S^3 + \delta_S\Delta\rho_S \ , \tag{15}$$

$$V_V = \alpha_V\rho_V + \gamma_V\rho_V^3 + \delta_V\Delta\rho_V \ , \tag{16}$$

$$V_{TS} = \alpha_{TS}\rho_{TS} \ , \text{ and} \tag{17}$$

$$V_{TV} = \alpha_{TV}\rho_{TV} \ , \tag{18}$$

where Eq. (15) is the isoscalar-scalar potential corresponding to σ meson (fictitious) exchange, Eq. (16) is the isoscalar-vector potential corresponding to ω meson exchange, Eq. (17) is the isovector-scalar potential corresponding to δ meson exchange, and Eq. (18) is the isovector-vector potential corresponding to ρ meson exchange. In these latter equations the scalar density is given by $\rho_S = \langle\phi|\bar{\psi}\psi|\phi\rangle$, the vector density is given by $\rho_V = \langle\phi|\bar{\psi}\gamma_0\psi|\phi\rangle$, the isovector-scalar density is given by $\rho_{TS} = \langle\phi|\bar{\psi}\tau_3\psi|\phi\rangle$, and the isovector-vector density is given by $\rho_{TV} = \langle\phi|\bar{\psi}\tau_3\gamma_0\psi|\phi\rangle$. These densities can of course be rewritten in terms of the upper and lower components of the Dirac wave functions (g_α, f_α), respectively, where $\alpha = \{n_r, \kappa, m\}$. For example, the vector (baryon) density becomes

$$\rho_V(r) = \sum_\alpha^{occ.} \frac{2j+1}{4\pi}[g_\alpha^2(r) + f_\alpha^2(r)] \ , \tag{19}$$

while the scalar density becomes

$$\rho_S(r) = \sum_{\alpha}^{occ.} \frac{2j+1}{4\pi}[g_\alpha^2(r) - f_\alpha^2(r)] \; . \tag{20}$$

The nine coupling constants of the Lagrangian were determined in a self-consistent procedure that solves the Dirac-Hartree equations for several nuclei simultaneously in a nonlinear least-squares adjustment algorithm of Levenberg-Marquardt type with respect to well-measured nuclear ground-state observables. The well-measured observables used (in order of decreasing experimental accuracy) are (a) the ground-state masses (binding energies), (b) the rms charge radii, and (c) the spin-orbit splittings of the least-bound neutron and proton spin-orbit pairs. We chose these observables for ten spherical closed-shell nuclei ranging from ^{16}O to ^{208}Pb in the determination of the coupling constants (40 observables to determine 9 coupling constants). The final coupling constants [9] are given in Table I where the first four refer to Eq. (12), the next three refer to Eq. (13), and the remaining two refer to Eq. (14). They span 13 orders of magnitude, but seven of them and the sum of the remaining two are *natural* (dimensionless numbers of order 1) when scaled in accordance with QCD mass scales and taking into account the constraint of chiral symmetry [9,12]. They should be viewed as an interim set of coupling constants in the development of the relativistic point coupling model. Note that the initial set of coupling constants determined with this approach appears in Ref. [8].

With these nine coupling constants one can calculate the following for spherical closed-shell nuclei: (a) Dirac single-nucleon wave functions and eigenvalues for both protons and neutrons, (b) nuclear ground-state mass and binding energy, (c) proton and neutron densities and their moments, (d) nuclear charge density and its moments, and (e) isoscalar- and isovector-, scalar and vector, potentials.

IV. CASE STUDY

For our present purpose we consider the upper and lower components of the Dirac single-nucleon wave functions for ^{208}Pb. Using the coupling constants of Table I we have calculated

the single-neutron wave functions for the occupied orbits in the ground state of this nucleus; these orbits have six neutron pseudo-spin doublets. Their properties are listed in Table II. Similarly, we have calculated the single-proton wave functions for the occupied orbits in the ground state of the same nucleus which contain four proton pseudo-spin doublets, and their properties are listed in Table III. The pseudo-spin doublets are ordered in the two tables according to increasing orbital angular momentum $\tilde{\ell}$ of the lower Dirac component $f_{n_r,\kappa}$, for each value of the radial quantum number n_r. The energy eigenvalues therein, $\varepsilon_{n_r,\kappa}$, in units of MeV, are related to the dimensionless energy eigenvalues $E_{n_r,\kappa}$, by

$$\varepsilon_{n_r,\kappa} = E_{n_r,\kappa}\, mc^2 \tag{21}$$

where mc^2 is either the free neutron mass or the free proton mass.

The upper and lower components of the Dirac wave functions for the most deeply bound neutron and proton pseudo-spin doublets (first entries in Tables II and III, respectively) are shown in Figs. 1 – 4. In Figs. 2 and 4 the lower components of the doublets are plotted with opposite sign so as to directly test Eq. (10), the pseudo-spin limit, against the observed (calculated) pseudo-spin breaking. It is clear that Eq. (10) is crudely satisfied when the eigenvalues are crudely degenerate (to within ~ 3 MeV for both neutrons and protons in this example). Comparisons of Figs. 1 and 2, for neutrons, and Figs. 3 and 4, for protons, show that while the upper components of the total Dirac wave function dominate, the lower components are certainly not negligible, and approximate, although crude in this example, pseudo-spin symmetry exists for both protons and neutrons.

We examine the systematics of pseudo-spin symmetry and the corresponding relativistic wave functions by considering the six neutron pseudo-spin doublets in Table II. Figures 5 – 7 show the lower components of three of the remaining five doublets. In Figs. 5 and 6, for $\tilde{\ell} = 2$ and 4, respectively, the pseudo-spin limit given by Eq. (10) is again approximately satisfied to about the same degree as that for the first neutron pseudo-spin doublet for $\tilde{\ell} = 1$ shown in Fig. 2. The same remark applies to the case for $\tilde{\ell} = 3$ (not shown). The four doublets all have the same radial quantum number $n_r = 1$, and have increasing orbital

angular momentum $\tilde{\ell}$ of the lower component. Figure 7 shows the lower components for the first of the two neutron pseudo-spin doublets that have radial quantum number $n_r = 2$. Here there is dramatic improvement in pseudo-spin symmetry, as expected [1] because these states are less bound and exact pseudo-spin symmetry occurs for *no bound* Dirac valence states. The same is true for the second neutron pseudo-spin doublet with $n_r = 2$ in Table II (not shown). A related systematic is that if the Dirac single-nucleon states of the pseudo-spin doublets of Tables II and III are sorted by classical major oscillator shells, then for those states in the same major shell, the energy splitting of the doublets decreases as $\tilde{\ell}$ decreases. In Table II, the $(n_r, \tilde{\ell})$ = (1,3) and (2,1) doublets are in the $N = 4$ major shell and the (1,4) and (2,2) doublets are in the $N = 5$ major shell. In both cases the energy splitting decreases with decreasing $\tilde{\ell}$. The same is true for the (1,3) and (2,1) doublets in Table III also corresponding to the $N = 4$ major shell. This point becomes more clear in Fig. 8 which shows the spectra for the twelve states making up the six neutron doublets and the eight states making up the four proton doublets. Clearly, for the doublets with the same pseudo-orbital angular momentum, the splitting between doublets decreases as the binding energy decreases, or, equivalently, as the radial quantum number increases. Also for doublets with different pseudo-orbital angular momentum, but roughly the same binding energy, say for example, $(n_r, \tilde{\ell})$ = (1,3) and (2,1), and $(n_r, \tilde{\ell})$ = (1,4) and (2,2), the doublet with the lower $\tilde{\ell}$ has the smaller energy splitting. These features are seen in the square well potential as in Equation (19) in [1] in which the energy splitting between the doublets is proportional to $2\tilde{\ell} + 1$ and E. The six neutron pseudo-spin doublet splittings of Fig. 8 are again plotted in Fig. 9, with the factor $(2\tilde{\ell} + 1)$ divided out, *vs* the mean eigenvalue $< \varepsilon >$ for each doublet. Here it is clearly quantitative that the energy splitting decreases as the binding energy decreases.

Finally, we compare two calculated neutron pseudo-spin doublets with experiment in Table II and two calculated proton pseudo-spin doublets with experiment in Table III. For both protons and neutrons, the magnitudes of the calculated eigenvalues and corresponding

measured values are comparable and the calculated energy splittings agree to within a factor $\sim$2 with the measured energy splittings in each of the four cases. The calculated splittings are always larger than the measured splittings which is not very surprising as most bound-state single-nucleon eigenvalue calculations, in relativistic mean field approaches, share the common feature of "spread-out eigenvalues" (see, for example, Ref. [7,8]) and our interim coupling constants (Table I) provide no exception. In addition, the measured and calculated states making up the neutron $(n_r, \tilde{\ell}) = (2,2)$ pseudo-spin doublet in Table II are reversed, a feature also occurring in other relativistic calculations [7,8]. On the other hand, the measured and calculated states making up the neutron (1,4) pseudo-spin doublet in the same table are not reversed in our calculation, but are reversed in other recent non-relativistic calculations [13,14]. We remark here that these latter features do not change our observations as to the connections between (approximate) pseudo-spin symmetry and the corresponding Dirac single-nucleon wave functions and eigenvalues.

V. CONCLUSIONS

We have shown that physically realistic relativistic mean fields lead to small pseudo-spin symmetry breaking which implies that the lower components of the corresponding Dirac single-nucleon wave functions satisfy

$$f_{-\tilde{\ell}}(r) \simeq -f_{\tilde{\ell}+1}(r) \tag{22}$$

where the pseudo-orbital angular momentum $\tilde{\ell}$ is exactly conserved in the pseudo-spin limit. Near this limit the lower components depend only upon $\tilde{\ell}$ (for fixed radial quantum number n_r) and the energy splitting between the doublets is small. Furthermore the pseudo-spin symmetry becomes increasingly valid as the pseudo-orbital angular momentum $\tilde{\ell}$ decreases and as the binding energy $E_{\tilde{\ell}}$ decreases (or as the radial quantum number n_r increases). These observations and conclusions are based upon our calculations of ten pseudo-spin doublets occurring in ^{208}Pb of which four have been measured and compare reasonably well

with the corresponding calculated doublets. Thus this work confirms the contention of Ref. [1] that pseudo-spin symmetry in nuclei arises largely from nucleons moving in relativistic mean fields with attractive isoscalar-scalar and repulsive isoscalar-vector components that are nearly equal in magnitude.

VI. ACKNOWLEDGMENTS

This research was supported by the United States Department of Energy.

*Electronic address: gino@t5.lanl.gov

†Electronic address: dgm@lanl.gov

REFERENCES

[1] J. N. Ginocchio, Phys. Rev. Lett. **78**, 436 (1997).

[2] K.T. Hecht and A. Adler, Nucl. Phys.**A137**, 129 (1969).

[3] A. Arima, M. Harvey, and K. Shimizu, Phys. Lett.**B30**, 517 (1969).

[4] A. Bohr, I. Hamamoto and B. R. Mottelson, Phys. Scripta **26**, 267 (1982).

[5] B. Mottelson, Nucl. Phys. **A522**, 1 (1991).

[6] D. Troltenier, C. Bahri, and J. P. Drayer, Nucl. Phys. **A586**, 53 (1995).

[7] B. D. Serot and J. D. Walecka, *The Relativistic Nuclear Many - Body Problem* in *Advances in Nuclear Physics*, edited by J. W. Negele and E. Vogt, Vol. **16** (Plenum, New York, 1986).

[8] B. A. Nikolaus, T. Hoch, and D. G. Madland, Physical Review **C46**, 1757 (1992).

[9] D. G. Madland, in *Proceedings of the International Conference on Nuclear Data for Science and Technology*, Trieste, Italy, May 19–24, 1997 (in press). [See Table 4, Calculation (b), and discussion.]

[10] T. D. Cohen, R. J. Furnstahl, and D. K. Griegel, Physical Review Lett. **67**, 961 (1991).

[11] W. Greiner, B. Müller, and J. Rafelski, *Quantum Electrodynamics of Strong Fields* (Springer-Verlag, New York, 1985).

[12] J. L. Friar, D. G. Madland, and B. W. Lynn, Phys. Rev. C **53**, 3085 (1996).

[13] R. B. Firestone *Table of Isotopes, Eighth Edition* (Wiley, New York, 1996) Vol. II, p. H-9,H-10.

[14] P. Möller, J. R. Nix, and K. -L. Kratz, At. Data Nucl. Data Tables **66**, 131 (1997) and P. Möller (private communication).

[15] M. R. Schmorak, Nuclear Data Sheets **43**, 383 (1984).

TABLES

TABLE I. Optimized Coupling Constants for the Interim Relativistic Point Coupling Model

Coupling Constant	Magnitude	Dimension
α_S	-4.517$\times10^{-4}$	MeV^{-2}
α_{TS}	-2.168$\times10^{-5}$	MeV^{-2}
α_V	3.435$\times10^{-4}$	MeV^{-2}
α_{TV}	5.365$\times10^{-5}$	MeV^{-2}
β_S	1.137$\times10^{-11}$	MeV^{-5}
γ_S	5.731$\times10^{-17}$	MeV^{-8}
γ_V	-4.423$\times10^{-17}$	MeV^{-8}
δ_S	-4.282$\times10^{-10}$	MeV^{-4}
δ_V	-1.155$\times10^{-10}$	MeV^{-4}

TABLE II. Calculated and Measured Neutron Pseudo-Spin Doublets in ^{208}Pb

$\tilde{\ell}$	$n_r, \kappa< 0$	(ℓ, j)	$\varepsilon_{n_r,\kappa<0}$ (MeV)	$n_r-1, \kappa> 0$	$(\ell+2, j+1)$	$\varepsilon_{n_r-1,\kappa>0}$ (MeV)
1	1, -1	$(s_{1/2})$	42.139	0, 2	$(d_{3/2})$	45.331
2	1, -2	$(p_{3/2})$	31.454	0, 3	$(f_{5/2})$	35.490
3	1, -3	$(d_{5/2})$	20.981	0, 4	$(g_{7/2})$	24.741
4	1, -4	$(f_{7/2})$	10.944	0, 5	$(h_{9/2})$	13.519
4	1, -4	$(f_{7/2})$	9.708[a]	0, 5	$(h_{9/2})$	10.781[a]
1	2, -1	$(s_{1/2})$	18.129	1, 2	$(d_{3/2})$	19.002
2	2, -2	$(p_{3/2})$	7.656	1, 3	$(f_{5/2})$	8.353
2	2, -2	$(p_{3/2})$	8.266[a]	1, 3	$(f_{5/2})$	7.938[a]

[a]Experimental value from Ref. [15].

TABLE III. Calculated and Measured Proton Pseudo-Spin Doublets in ^{208}Pb

$\tilde{\ell}$	$n_r, \kappa< 0$	(ℓ, j)	$\varepsilon_{n_r,\kappa<0}$ (MeV)	$n_r - 1, \kappa> 0$	$(\ell + 2, j + 1)$	$\varepsilon_{n_r-1,\kappa>0}$ (MeV)
1	1, -1	$(s_{1/2})$	32.047	0, 2	$(d_{3/2})$	35.830
2	1, -2	$(p_{3/2})$	21.800	0, 3	$(f_{5/2})$	26.358
3	1, -3	$(d_{5/2})$	11.597	0, 4	$(g_{7/2})$	15.930
3	1, -3	$(d_{5/2})$	9.696[a]	0, 4	$(g_{7/2})$	11.487[a]
1	2, -1	$(s_{1/2})$	8.416	1, 2	$(d_{3/2})$	9.663
1	2, -1	$(s_{1/2})$	8.013[a]	1, 2	$(d_{3/2})$	8.364[a]

[a]Experimental value from Ref. [15].

FIGURES

FIG. 1. Dirac upper component wave functions for the neutron pseudo-spin doublet $(n_r, \tilde{\ell}) =$ (1,1) in ^{208}Pb and specified more completely in the first line of Table II.

FIG. 2. Dirac lower component wave functions corresponding to Fig. 1. The sign of the component with $\kappa > 0$ has been reversed to test Eq. (10).

FIG. 3. Dirac upper component wave functions for the proton pseudo-spin doublet $(n_r, \tilde{\ell}) =$ (1,1) in ^{208}Pb and specified more completely in the first line of Table III.

FIG. 4. Dirac lower component wave functions corresponding to Fig. 3. The sign of the component with $\kappa > 0$ has been reversed to test Eq. (10).

FIG. 5. Dirac lower component wave functions for the neutron pseudo-spin doublet $(n_r, \tilde{\ell})$ = (1,2) in ^{208}Pb and specified more completely in the second line of Table II. The sign of the component with $\kappa > 0$ has been reversed to test Eq. (10).

FIG. 6. The same as Fig. 5 except for the pseudo-spin doublet $(n_r, \tilde{\ell}) =$ (1,4) and specified more completely in the fourth line of Table II.

FIG. 7. The same as Fig. 5 except for the pseudo-spin doublet $(n_r, \tilde{\ell}) =$ (2,1) and specified more completely in the sixth line of Table II.

FIG. 8. Spectra of the six neutron and four proton pseudo-spin doublets occurring in ^{208}Pb. Note that the pseudo-spin symmetry is more valid for the higher value of the radial quantum number.

FIG. 9. Dirac energy splittings of the six neutron pseudo-spin doublets shown in Fig. 8, normalized by $(2\tilde{\ell} + 1)$, *vs* the mean energy eigenvalue $< \varepsilon >$ of the doublet. The line is a linear fit to the four cases with $n_r = 1$.

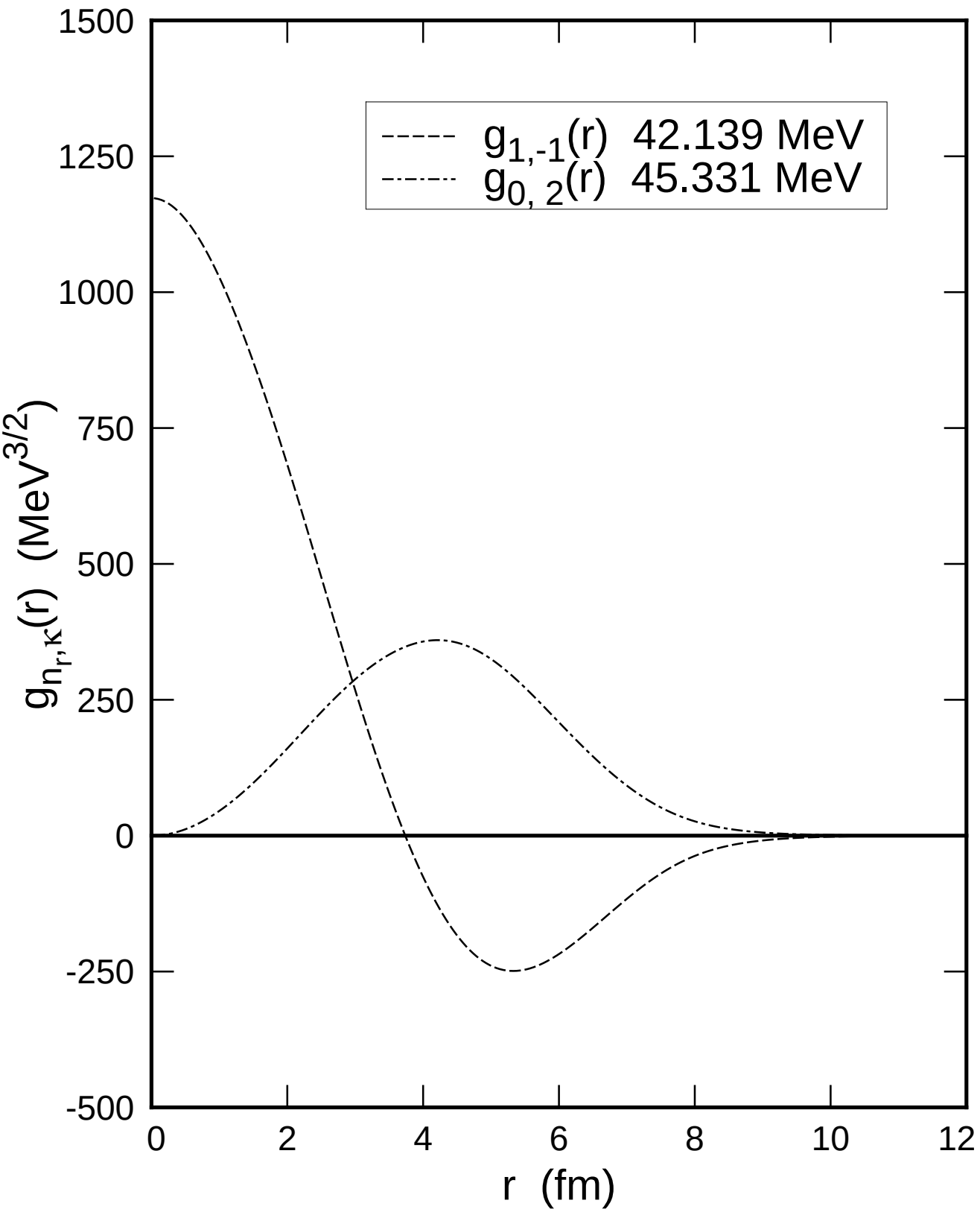
Dirac Single-Nucleon Wave Functions
(neutron upper components for 208Pb)
g1,-1(r) 42.139 MeV
g0, 2(r) 45.331 MeV
gnr,κ(r) (MeV3/2)
r (fm)
1500
1250
1000
750
500
250
0
-250
-500
0
2
4
6
8
10
12

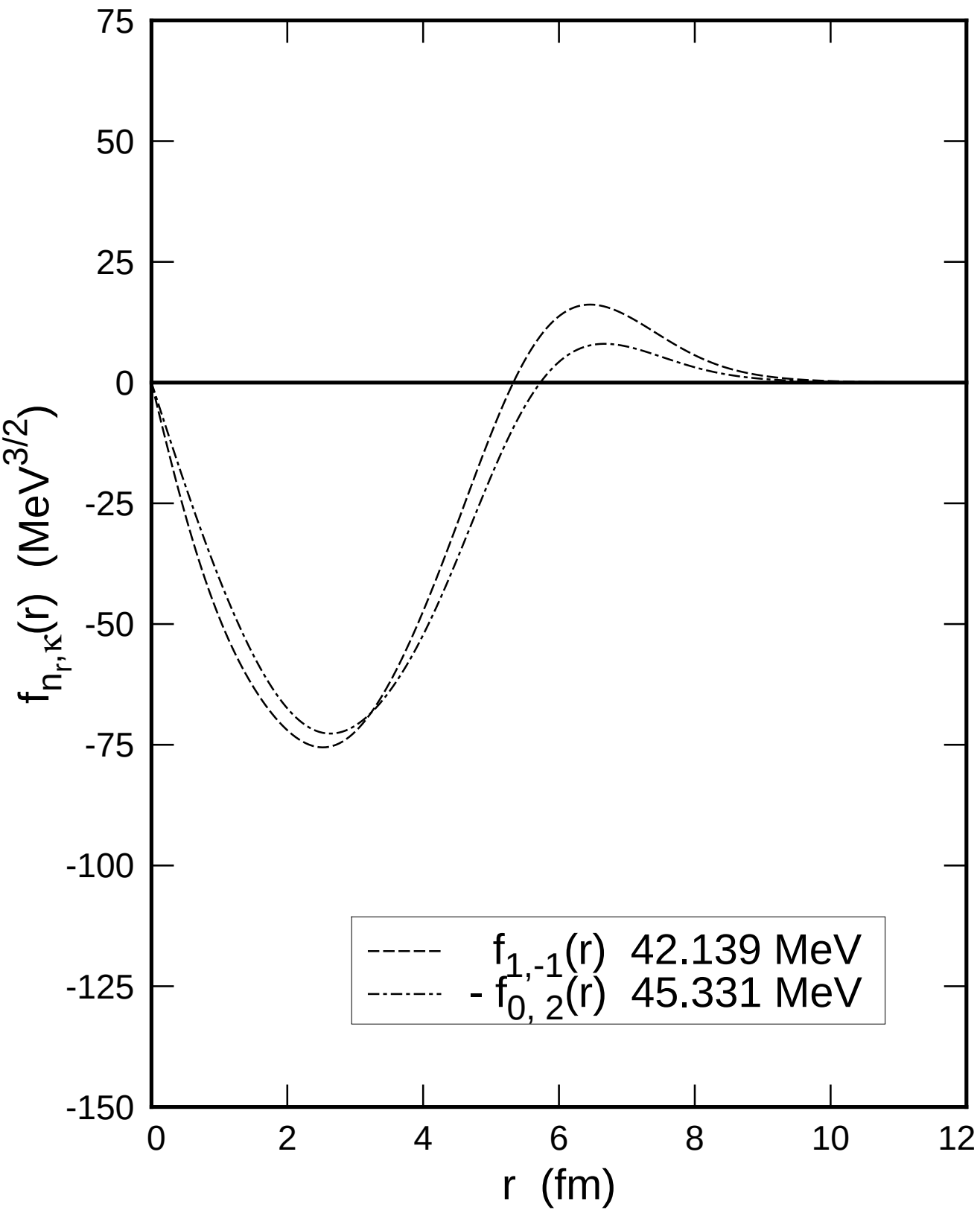
Dirac Single-Nucleon Wave Functions
(neutron lower components for 208Pb)
75
50
25
0
-25
-50
-75
-100
-125
-150
0
2
4
6
8
10
12
r (fm)
f_{n_r,κ}(r) (MeV^{3/2})
f_{1,-1}(r) 42.139 MeV
- f_{0,2}(r) 45.331 MeV

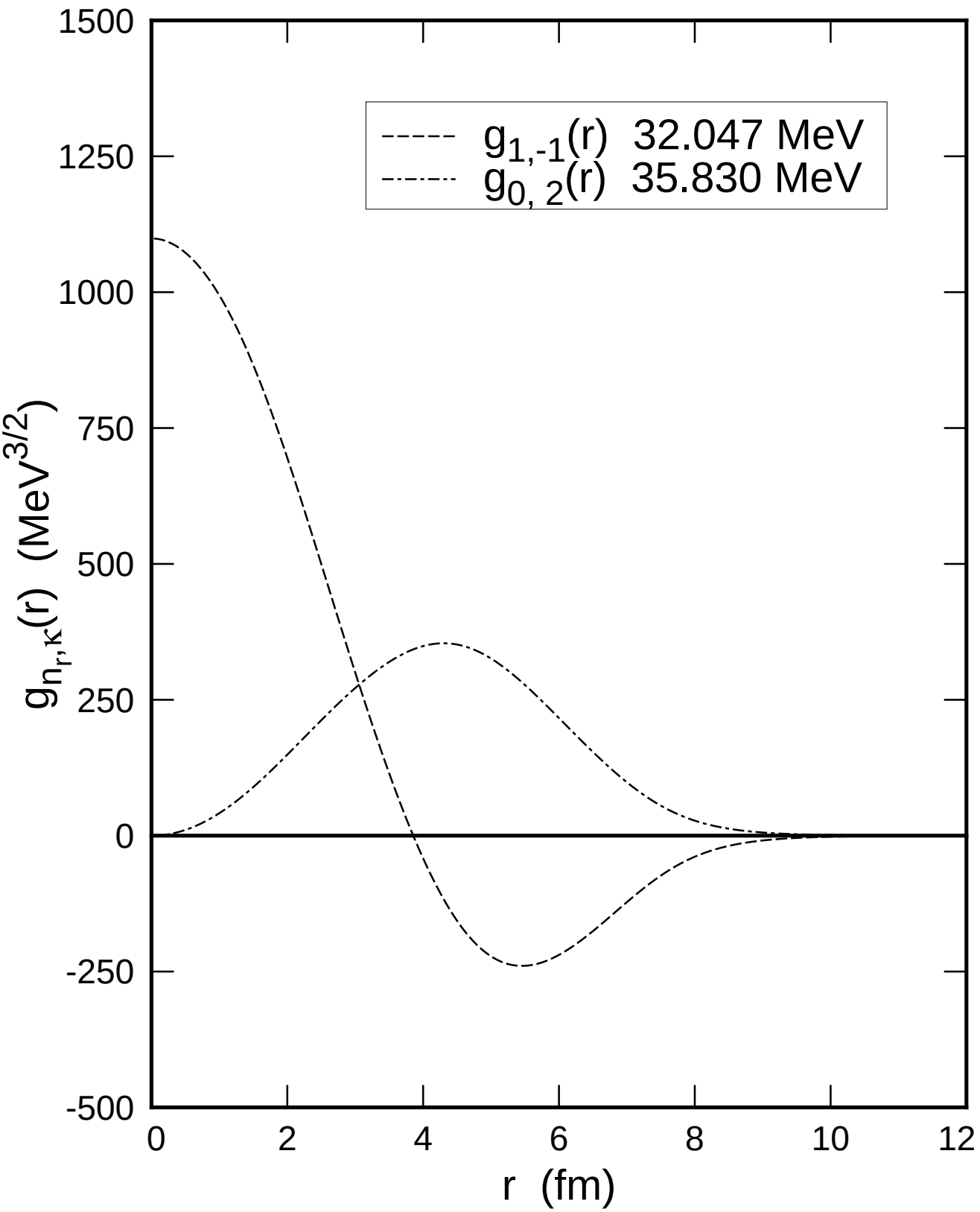
Dirac Single-Nucleon Wave Functions
(proton upper components for 208Pb)
g1,-1(r) 32.047 MeV
g0, 2(r) 35.830 MeV
gnr,κ(r) (MeV3/2)
r (fm)
1500
1250
1000
750
500
250
0
-250
-500
0
2
4
6
8
10
12

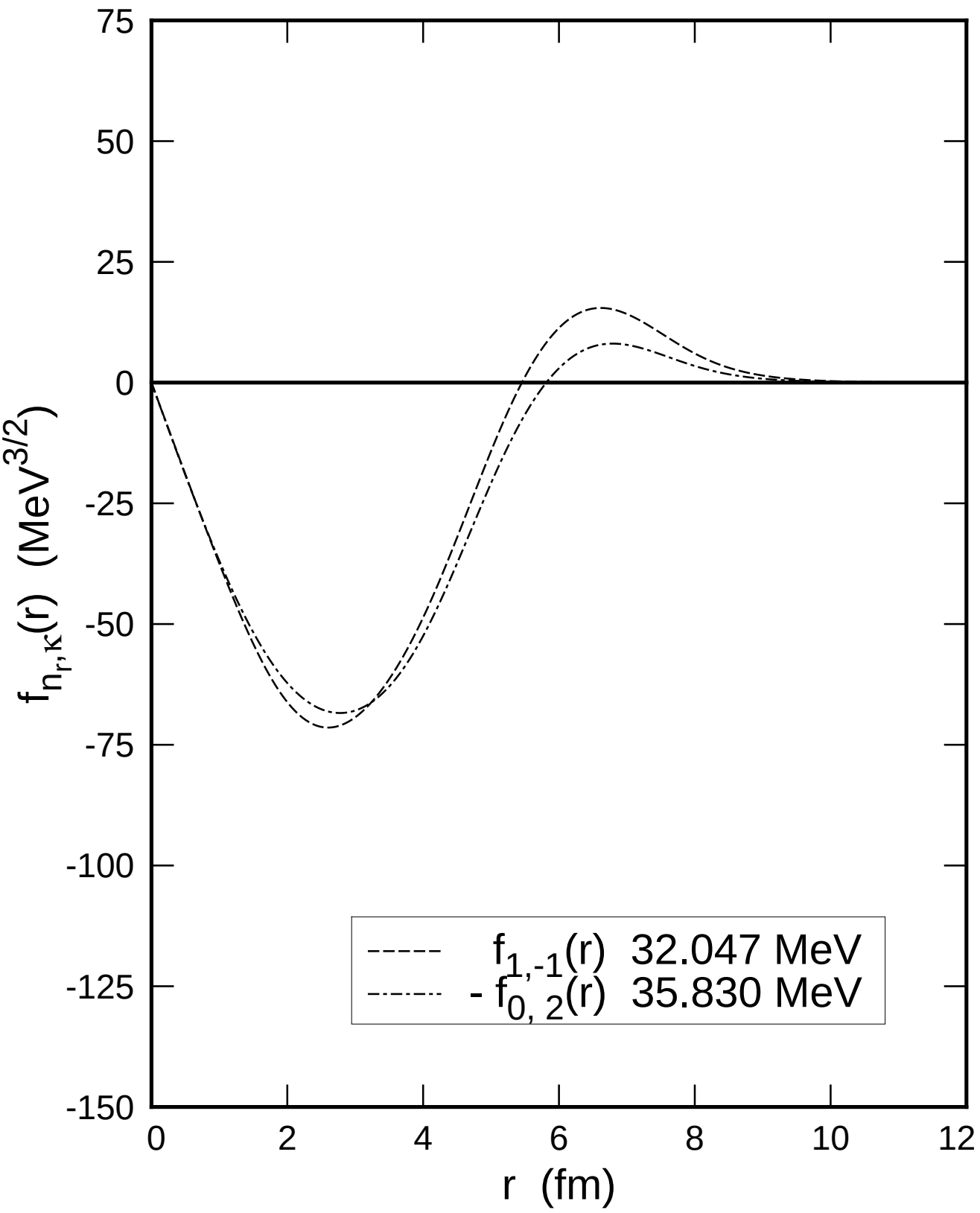
Dirac Single-Nucleon Wave Functions
(proton lower components for 208Pb)
75
50
25
0
-25
-50
-75
-100
-125
-150
0
2
4
6
8
10
12
r (fm)
f_{n_r,κ}(r) (MeV^{3/2})
f_{1,-1}(r) 32.047 MeV
- f_{0,2}(r) 35.830 MeV

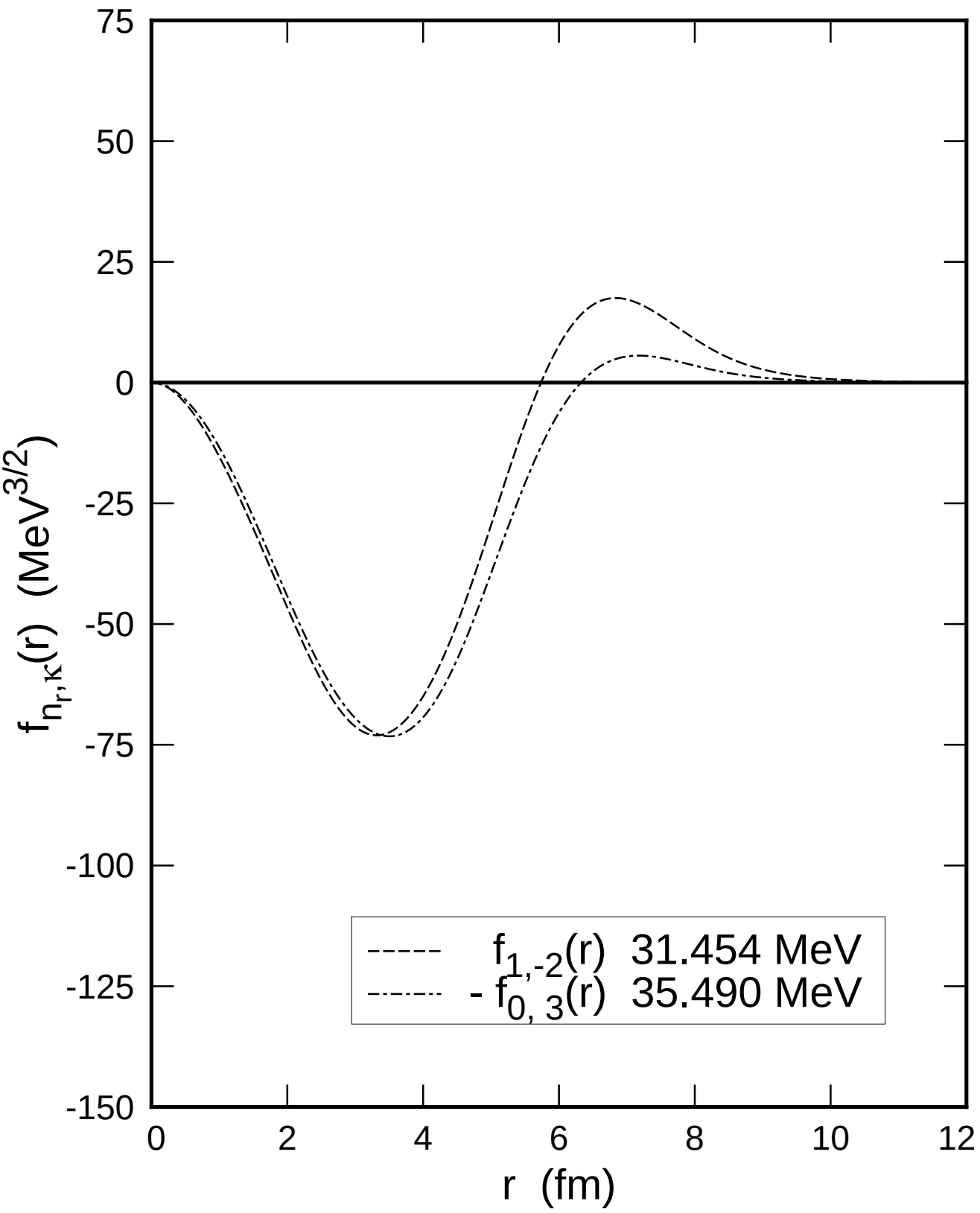
Dirac Single-Nucleon Wave Functions
(neutron lower components for 208Pb)
75
50
25
0
-25
-50
-75
-100
-125
-150
0
2
4
6
8
10
12
r (fm)
f_{n_r,κ}(r) (MeV^{3/2})
f_{1,-2}(r) 31.454 MeV
- f_{0,3}(r) 35.490 MeV

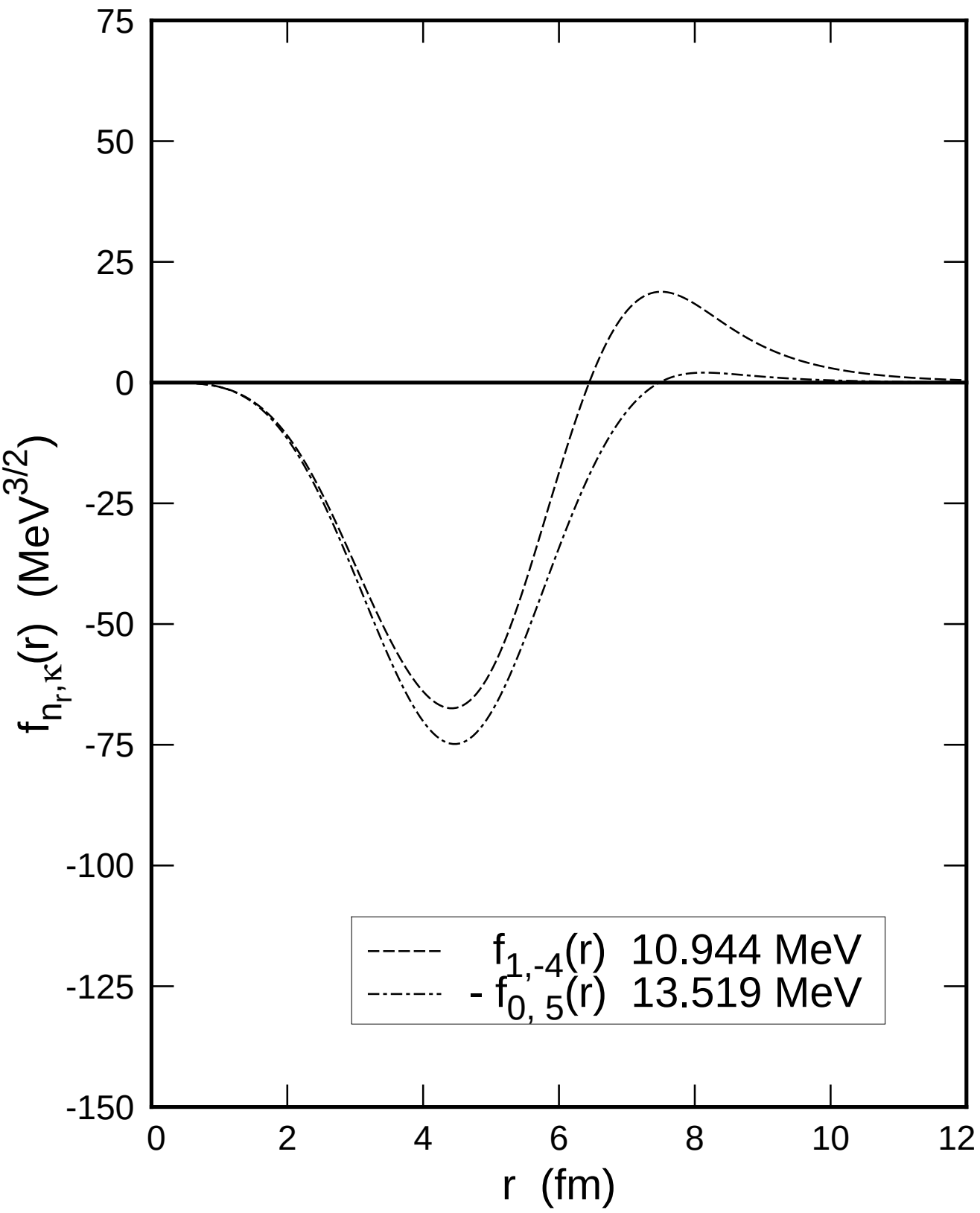
Dirac Single-Nucleon Wave Functions
(neutron lower components for 208Pb)
75
50
25
0
-25
-50
-75
-100
-125
-150
0
2
4
6
8
10
12
r (fm)
f_{n_r,κ}(r) (MeV^{3/2})
f_{1,-4}(r) 10.944 MeV
- f_{0,5}(r) 13.519 MeV

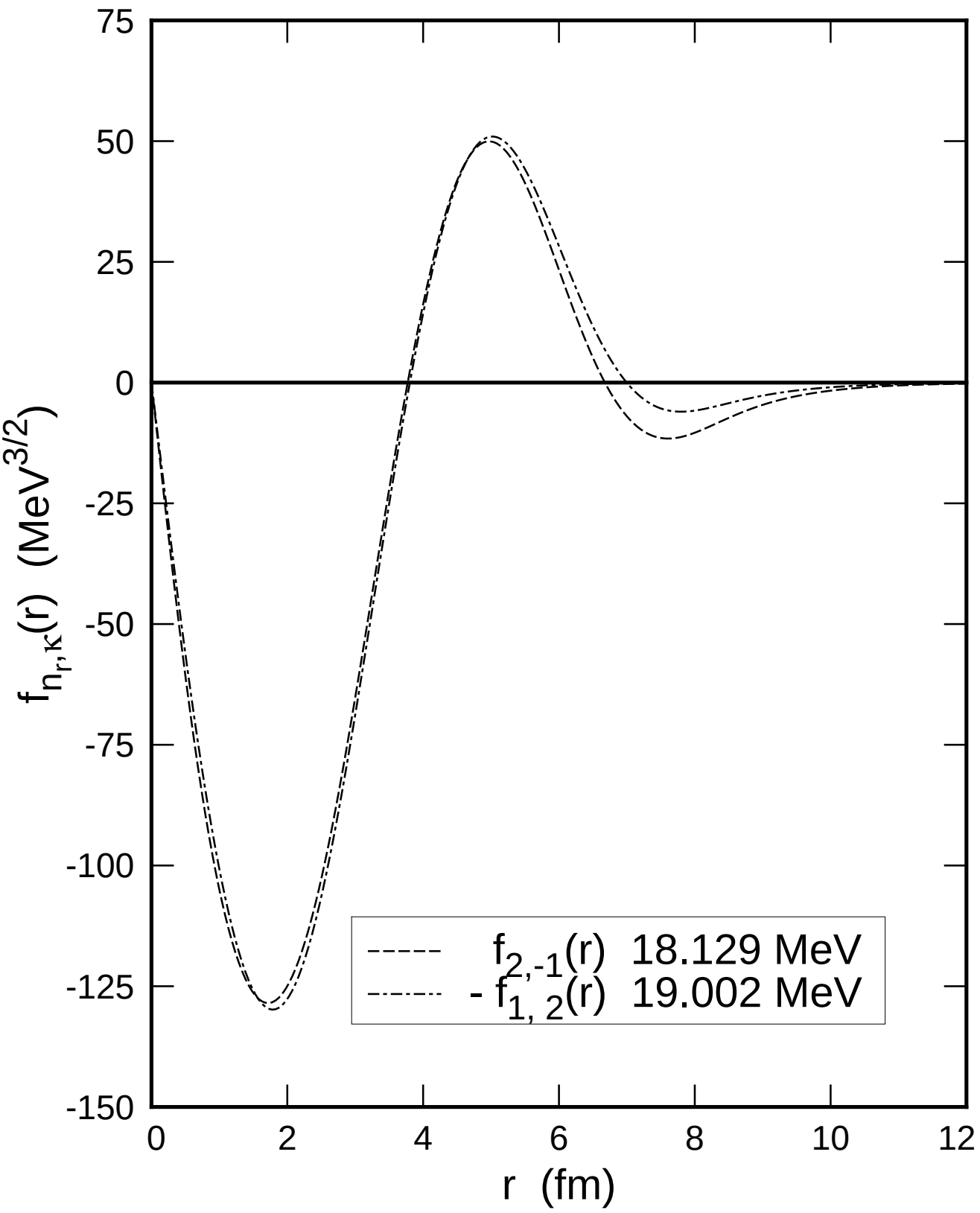
Dirac Single-Nucleon Wave Functions
(neutron lower components for 208Pb)
75
50
25
0
-25
-50
-75
-100
-125
-150
0
2
4
6
8
10
12
r (fm)
f_{n_r,κ}(r) (MeV^{3/2})
f_{2,-1}(r) 18.129 MeV
- f_{1,2}(r) 19.002 MeV

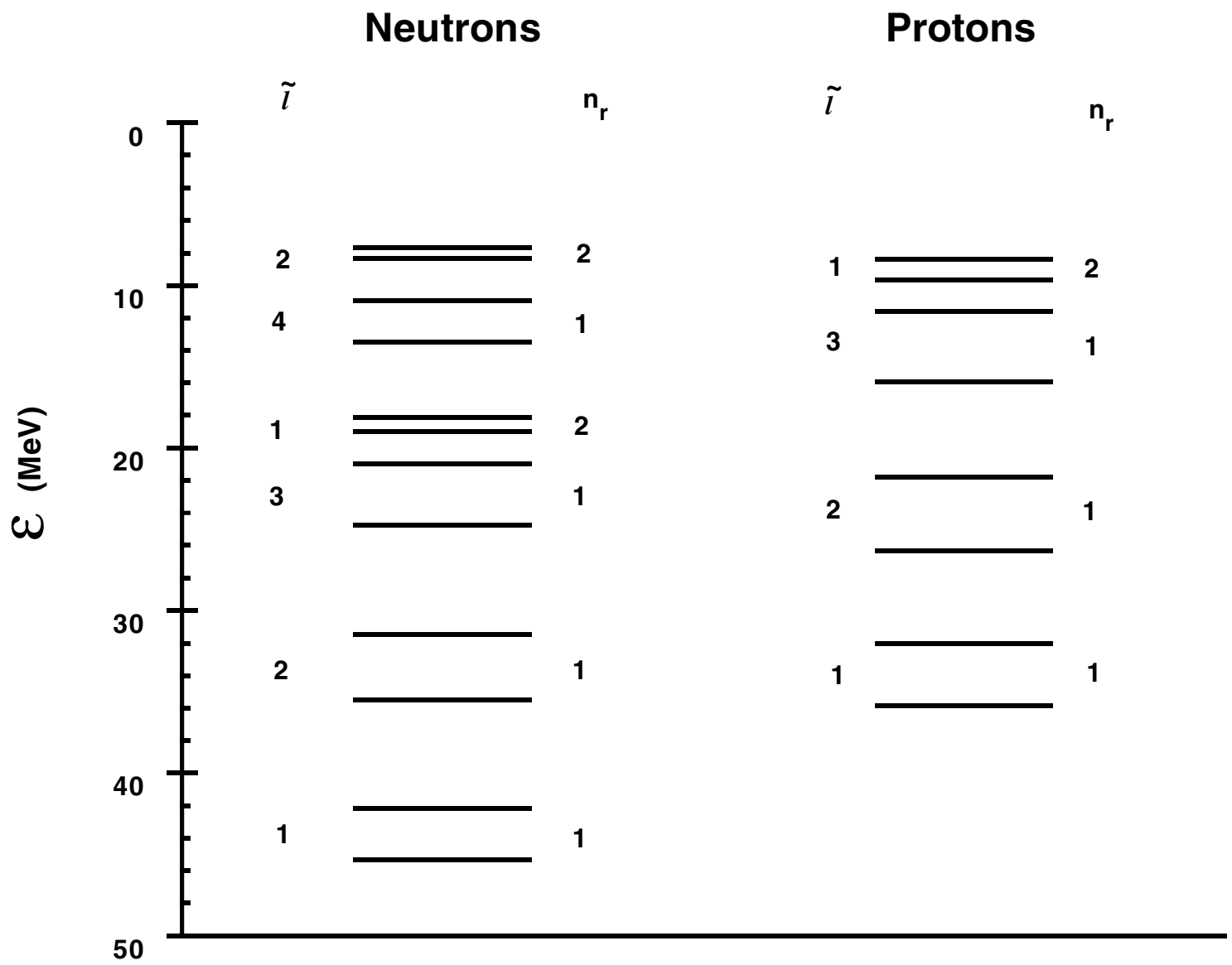
Neutrons
Protons
$\tilde{l}$
n_r
ε (MeV)
0
10
20
30
40
50
2
4
1
3
2
1
2
1
1
2
1
3
2
1
1
2
1
1

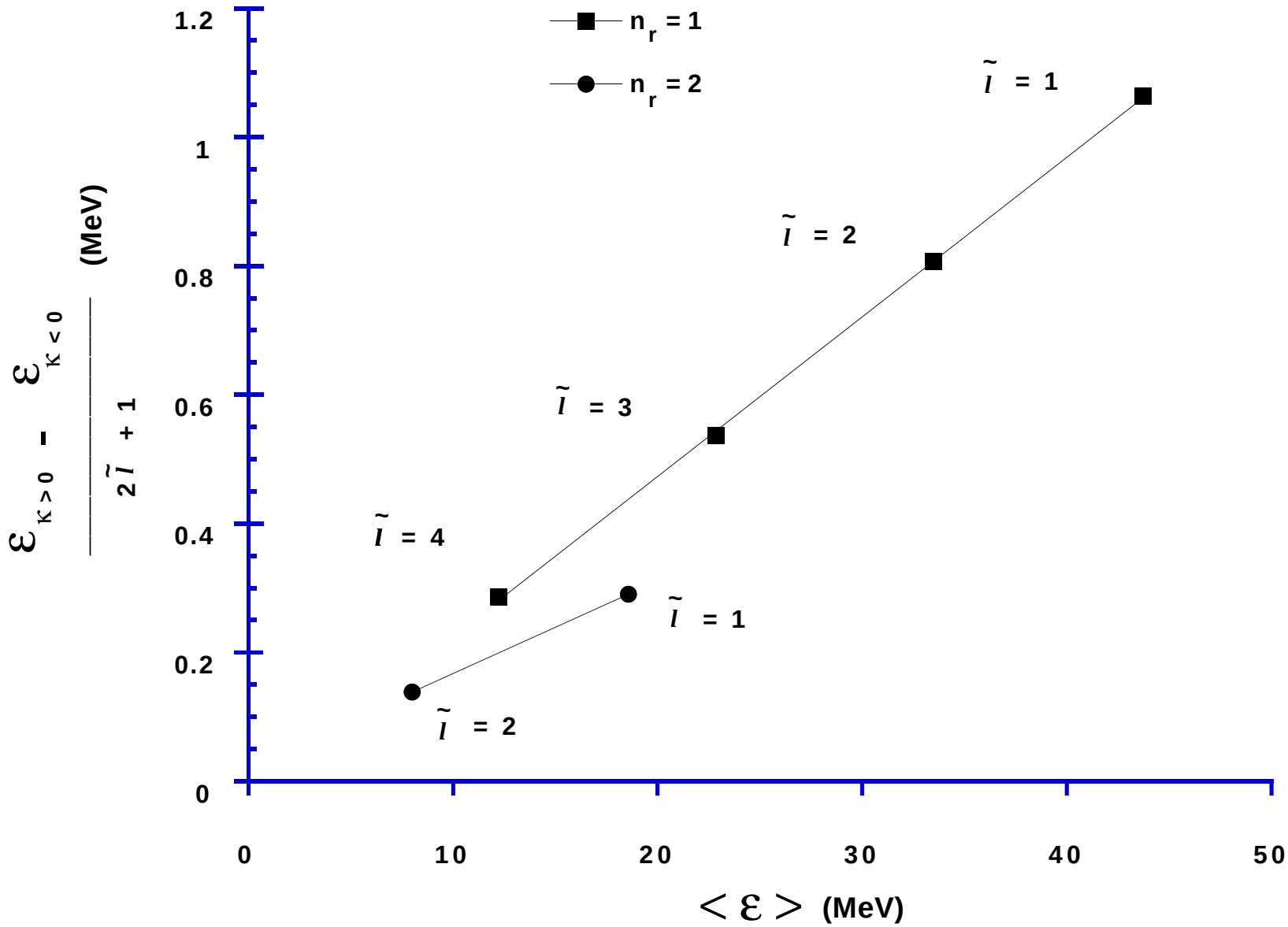
1.2
1
0.8
0.6
0.4
0.2
0
0
10
20
30
40
50
$n_r = 1$
$n_r = 2$
$\tilde{l} = 1$
$\tilde{l} = 2$
$\tilde{l} = 3$
$\tilde{l} = 4$
$\tilde{l} = 1$
$\tilde{l} = 2$
$\frac{\varepsilon_{\kappa>0} - \varepsilon_{\kappa<0}}{2\tilde{l}+1}$ (MeV)
$\langle \varepsilon \rangle$ (MeV)